The following publication C. Yao, S. Gao, Y. Wang, P. Wang, W. Jin and W. Ren, "Silica Hollow-Core Negative Curvature Fibers Enable Ultrasensitive Mid-Infrared Absorption Spectroscopy," in Journal of Lightwave Technology, vol. 38, no. 7, pp. 2067-2072, 1 April, 2020 is available at https://doi.org/10.1109/JLT.2019.2960804.

Silica hollow-core negative curvature fibers enable ultrasensitive mid-infrared absorption spectroscopy

Chenyu Yao, Shoufei Gao, Yingying Wang, Pu Wang, Wei Jin, *Senior Member, IEEE*, Wei Ren

***Abstract*—Ultrasensitive mid-infrared absorption spectroscopy was demonstrated by the use of a novel silica-based hollow-core negative curvature fiber (HC-NCF). The HC-NCF used in this work consists of a single ring of six nontouching cladding capillaries around the hollow core, thus forming a unique core boundary with a negative curvature. Such a silica HC-NCF enables the broadband single-mode transmission in the mid-infrared. By using the HC-NCF as a compact gas cell, a proof-of-principle experiment was conducted to detect the N_2O line at 2778.37 cm^{-1} with a distributed-feedback interband cascade laser emitting at 3.6 μm. A minimum detectable absorbance of 3×10^{-5} was achieved for a fiber length of 120 cm, corresponding to a noise equivalent absorption (NEA) coefficient of 2.5×10^{-7} cm^{-1}. Silica HC-NCFs offer a new opportunity of developing sensitive and compact gas sensors using mid-infrared absorption spectroscopy.**

***Index Term*—Mid-infrared absorption spectroscopy, Gas sensor, Optical fiber sensor, Photonic crystal fiber, Hollow core fiber**

I. Introduction

Hollow-core microstructured optical fibers (HC-MOFs) typically comprise a glass microstructure with a tiny hollow core in the central region where light and gas/liquid samples could interact perfectly. Flexible HC-MOFs with a low optical transmission loss provide opportunities for developing sensitive and compact optical sensors that would otherwise be difficult for free-space optics. The use of HC-MOFs for gas sensing has been investigated by several spectroscopic methods such as direct absorption spectroscopy (DAS) [1-5], wavelength modulation spectroscopy (WMS) [6-8] and photothermal spectroscopy (PTS) [9,10].

This work is supported by General Research Fund from the University Grants Committee of the Hong Kong SAR, China (14206317). (*Corresponding author: Wei Ren*.)

Chenyu Yao and Wei Ren are with the Department of Mechanical and Automation Engineering, The Chinese University of Hong Kong, New Territories, Hong Kong SAR, China (e-mail: cyyao@mae.cuhk.edu.hk; renwei@mae.cuhk.edu.hk).

Shoufei Gao, Yingying Wang, and Pu Wang are with the Beijing Engineering Research Center of Laser Technology, Institute of Laser Engineering, Beijing University of Technology, Beijing 100124, China (jngaofei@gmail.com; wangyingying@bjut.edu.cn; wangpu@bjut.edu.cn).

W. Jin is with the Department of Electrical Engineering, The Hong Kong Polytechnic University, Hong Kong, and also with The Hong Kong Polytechnic University Shenzhen Research Institute, Shenzhen 518057, China (e-mail: wei.jin@polyu.edu.hk).

Previous HC-MOF-based gas sensors mostly employed the type of hollow-core photonic bandgap fiber (HC-PBF). Silica HC-PBFs normally have a limited spectral transmission below 2 μm due to the intrinsic absorption of fiber material at the mid-infrared region. Mid-infrared spectrum known as the molecular fingerprint region (2.5-10 μm) is more attractive for laser spectroscopy as a lot of molecules have the fundamental absorption bands in this spectral region. Only a few research groups have reported the HC-PBF-based gas detection in the mid-infrared. Kornaszewski *et al.* [1] conducted a proof-of-principle experiment for the mid-infrared (3.15-3.35 μm) measurement of 5% methane/nitrogen mixture using a 40-μm-core HC-PBF. Petrovich *et al.* [2] demonstrated the mid-infrared detection of ethane at 3.4 μm in a 50-μm-core HC-PBF using a supercontinuum source and a spectrum analyzer. With such a 5.69-m HC-PBF, they obtained a noise equivalent absorption (NEA) coefficient of 4.6×10^{-5} cm^{-1} which was mainly limited by the fiber mode noise. The mode interference arises from the fact that a large number of modes are propagating in the hollow-core fiber when the core diameter is above 20 μm [11].

Hollow-core negative curvature fibers (HC-NCFs), more broadly named hollow-core anti-resonant fiber, are recently emerging as a new type of HC-MOFs with nearly single-mode transmission, low optical loss and wide spectral range [12-15]. Particularly, HC-NCFs are designed with a new structure which normally consists of a single ring of silica capillaries around a hollow core, thus forming a unique core boundary with a negative curvature. The core-guided mode in the HC-NCF is prevented from coupling to the cladding due to the inhibited coupling between the core mode and other cladding modes. Additionally, a small gap is introduced between the neighboring capillary tubes to generate a nodeless boundary that is completely devoid of any connecting nodes and strongly favors the inhibited coupling [13].

A variety of hollow core fibers have been used for biochemical sensing [16-18] and gas sensing applications. By the use of such a HC-NCF of 1.35 m, Nikodem *et al.* [7] measured CO_2 using wavelength modulation spectroscopy. A detection limit of 5 ppm CO_2 was achieved at the wavelength of 2004 nm, corresponding to a NEA coefficient of 6.7×10^{-7} cm^{-1}. Recently, Yao *et al.* [10] reported the first photothermal CO sensor at 2327 nm using a HC-NCF and achieved a normalized noise equivalent absorption (NNEA) coefficient of 4.4×10^{-8}

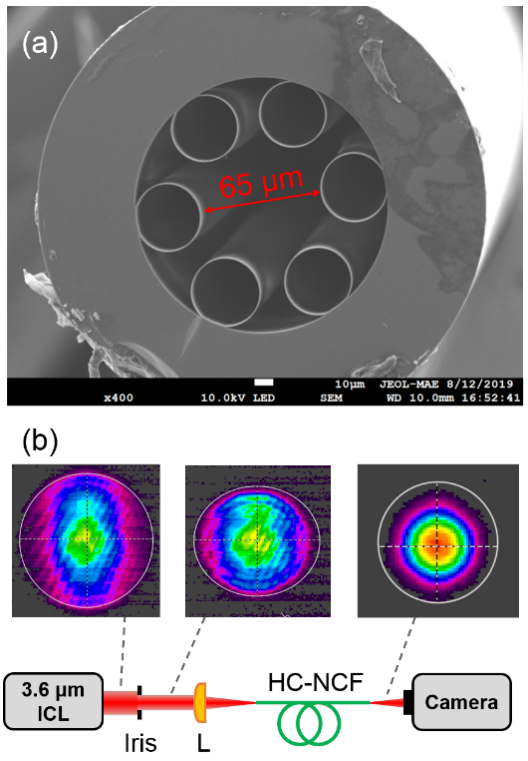

Fig. 1. (a) SEM image of the HC-NCF used in this work; (b) beam profiles of the 3.6 μm ICL before and after being coupled into the HC-NCF.

$cm^{-1}WHz^{-1/2}$. However, both studies exploited the weak overtone absorption bands of CO_2 and CO in the extended near-infrared range between 2 μm and 2.3 μm.

Silica HC-NCFs with mid-infrared transmission have been recently reported by a few research groups [19-22]. Yu *et al.* [19] developed a silica HC-NCF for the mid-infrared transmission from 2.9 μm to 3.8 μm with a minimum attenuation of 34 dB/km. Gao *et al.* [20] designed a nodeless HC-NCF for the infrared guidance between 1.6 μm and 3.4 μm. Due to the reduced overlap of the core mode with silica, these HC-NCFs exhibit a lower optical loss and broader transmission window than the previous HC-PBF counterparts [23-25]. Mid-infrared HC-NCFs have been demonstrated for supercontinuum generation [26,27] and fiber laser development [28,29]. However, no research has been reported on using mid-infrared HC-NCFs for gas sensing.

In this paper, we demonstrate the first mid-infrared gas sensor development using direct absorption spectroscopy with a HC-NCF. A distributed feedback (DFB) interband cascade laser (ICL) emitting at 3.6 μm is used to access the absorption line of nitrous oxide (N_2O) at 2778.37 cm^{-1} as a proof-of-principle. The HC-NCF used in this study has a hollow core diameter of 65 μm and consists of a single ring of six nontouching capillaries. We will discuss the coupling optics, optical noise and sensor performance in detail.

II. Spectroscopic Fundamentals

When the laser wavelength is scanned across the absorption line of the target gas, the transmitted laser intensity with gas absorption is monitored by a photodetector. The relationship between the incident laser intensity I_0 and the transmitted laser intensity I_t for a homogeneous absorbing medium is governed by the Beer-Lambert law:

$$I_t / I_0 = \exp(-k(\upsilon) \cdot L), \tag{1}$$

where k is the absorption coefficient and L is the path length in cm through the absorbing medium. The linear product of kL is known as the absorbance, α, that is given by

$$\alpha(\upsilon) = C \cdot P \cdot S \cdot \phi(\upsilon) \cdot L, \tag{2}$$

in which C is the species concentration, P is the total gas pressure in atm, S is the linestrength of the target transition in $cm^{-2}atm^{-1}$, υ is the laser wavelength in cm^{-1}, and $\phi(\upsilon)$ is the lineshape function of the transition.

The lineshape function $\phi(\upsilon)$ characterizes the probability distribution of the absorbance as a function of laser frequency [30]. The lineshape function is defined so that its integral over frequency is unity and peaks at the absorption line center υ_0. Therefore, the integrated area of absorbance under the absorption lineshape can be defined as (3):

$$A \equiv \int_{-\infty}^{+\infty} \alpha(\upsilon) d\upsilon = C \cdot P \cdot L \cdot S \tag{3}$$

The lineshape function could be derived from different broadening mechanisms including Doppler broadening, natural lifetime broadening and collisional broadening. Doppler broadening is characterized by the Gaussian lineshape ϕ_D, whereas the other two are given by the Lorentzian lineshape ϕ_L. In general, the overall broadening is a combination of different mechanisms, so the overall lineshape will be a convolution of the Gaussian and Lorentzian lineshape,

$$\phi(\upsilon) = \phi_V(\upsilon) = \int_{-\infty}^{+\infty} \phi_D(u) \phi_L(u - \upsilon) du, \tag{4}$$

where ϕ_V is called the Voigt lineshape function that could be represented by the numerical algorithm [31]. The absorbance at a specific spectral frequency can be written as:

$$\alpha(\upsilon) = A \times \phi_D(\upsilon_0) \phi_V(\upsilon). \tag{5}$$

III. Experimental

The HC-NCF used in this work consists of a single ring of six nontouching silica capillaries; see the scanning electron microscope (SEM) image of the cross section shown in Fig. 1(a). The hollow core has an inner diameter of 65 μm inscribed by those capillaries with a diameter of 34 μm and a strut thickness of 0.69 μm. This HC-NCF operates in its first anti-resonance band with a transmission bandwidth from 1.6 μm to mid-infrared [20]. We used such a HC fiber with a total length of 120 cm as a demonstration for mid-infrared gas

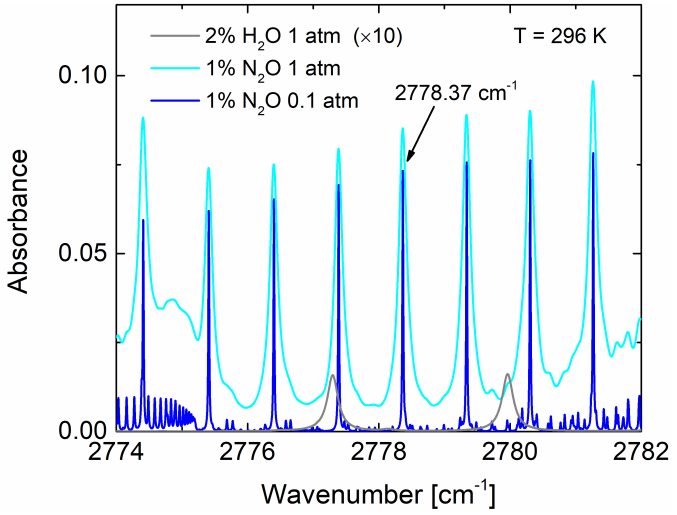

Fig. 2. Simulated absorption spectra of 1% N_2O and 2% H_2O at two different gas pressures (0.1 atm and 1 atm) within the scan range of the ICL between 2774 cm^{-1} and 2782 cm^{-1}. The H_2O absorption lines are magnified by 10 times.

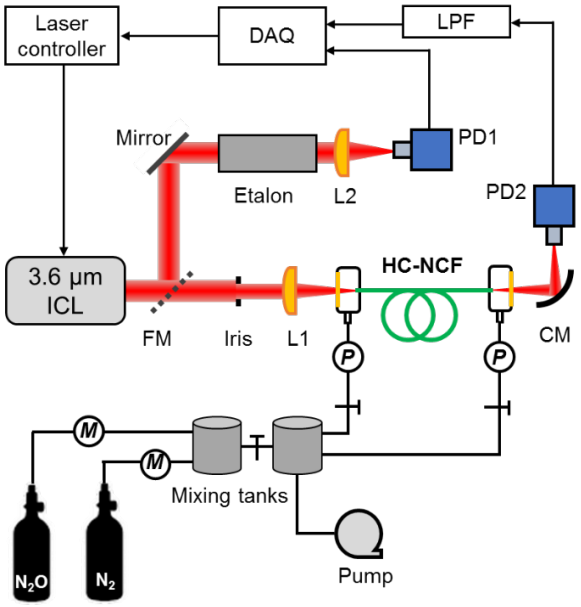

Fig. 3. Experimental setup of the DAS-based gas sensor using a HC-NCF. FM: flip mirror; L: lens; CM: concave mirror; PD: photodetector; P: pressure gauge; M: mass flow meter; LPF: low-pass filter.

sensing at the wavelength near 3.6 μm.

The ICL beam with an elliptical profile was coupled into the fiber by a CaF_2 lens (f = 50 mm) fixed on a XY-translation mount. An iris was placed in front of the focusing lens to reshape the laser beam shown in Fig. 1(b). The laser beam was focused to a spot size of roughly 45 μm at the fiber entrance that is 0.7 of the hollow core size. The incident and transmitted laser power through the HC-NCF was measured to be 2 mW and 1.1 mW, respectively. The coupling efficiency was about 66% based on an estimated fiber transmission loss 0.6 dB/m at the wavelength of 3.6 μm. A far-field image of the fiber output illustrated in Fig. 1(b) demonstrates the LP_{01} fundamental mode of the transmitted laser beam. The present HC-NCF exhibits a broader transmission band than that used previously for photothermal sensing [10]. The transmission band of HC-NCFs is mainly determined by the fiber parameters such as core diameter, capillary diameter, and strut thickness.

The ICL could be tuned between 2774 cm^{-1} and 2782 cm^{-1} to exploit N_2O absorption lines by adjusting the injection current [32]. Water vapor (H_2O) may be a possible interfering species due to the adsorption/desorption effects occurring on the inner surface of the fiber. Fig. 2 depicts the simulated absorption spectra of 1% N_2O at two representative pressures (0.1 atm and 1.0 atm) and 2% H_2O based on HITRAN database [33]. The weak absorption lines of H_2O are generally negligible, which were multiplied by 10 in the figure for a clear illustration. Several strong absorption lines of N_2O are observed in this spectral range. Note that the N_2O absorption peak at 2778.37 cm^{-1} is selected in the following DAS measurements. The ICL used in this work has a linewidth of ~ 3 MHz, which is two orders of magnitude smaller than the FWHM (full width at half maximum) of the target N_2O line at 0.1 atm.

Fig. 3 depicts the experimental setup of the HC-NCF-based absorption gas sensor. The two fiber ends were cleaved by a ruby scribe and then enclosed inside two compact gas cells (~5 cm^3 in volume) for gas loading and purging purposes. A CaF_2 window was installed on the gas cell for fiber coupling and optical access. The coupling optics were used the same as that shown in Fig. 1. The transmitted laser beam was collected by a concave mirror (f = 50 mm) onto a photodetector (Vigo Systems). When performing DAS measurements, a 10 Hz triangular wave (300 mV_{p-p}) was added to the laser driver (ILX Lightwave) to scan the laser frequency. The photodetector signal was filtered by an electronic low-pass filter ($f_{cut\text{-}off}$ = 1 kHz) and then acquired by the data acquisition card with a sampling rate of 20 kHz. After each DAS experiment, a flip mirror was used to direct the laser beam through a germanium etalon for calibrating laser wavelength [34].

The N_2O/N_2 mixtures were generated in a mixing tank connected with two gas cylinders. Before loading the gas sample, the hollow core fiber was first evacuated by a vacuum pump. Then the gas mixture was introduced into one of the gas cells. The gas mixture was pressurized into the fiber under a pressure difference of 1.5 atm between the two fiber ends. Finally, the gas flow was stopped to generate an expected gas pressure in the hollow core.

IV. Results and Discussion

A. Fringe noise analysis

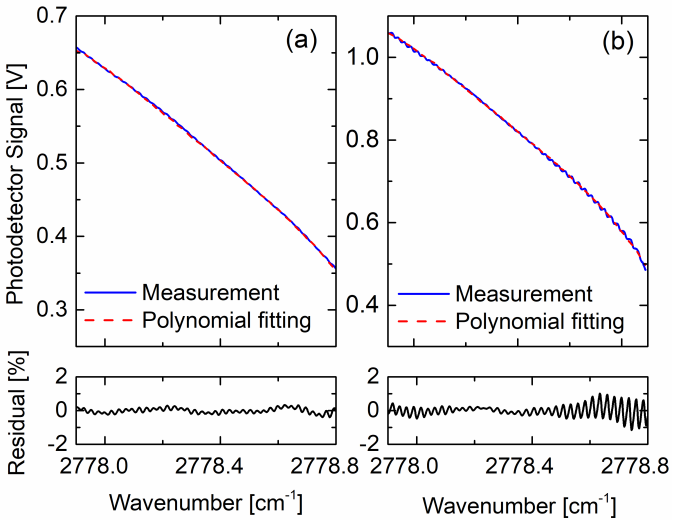

Fig. 4. ICL transmission signal through the HC-NCF filled with air for an iris aperture of (a) 5.2 mm and (b) 10 mm.

When the light is coupled into the hollow core, it is possible to excite both the fundamental mode and higher-order modes. All these core modes propagate through the fiber and then combine coherently at the fiber output to generate the mode interference [6,35]. Such a mode interference appears as a patterned, fringe-like noise in the detected transmission signal by a photodetector.

The mode interference increases with the number of the total higher-order modes supported in the fiber. A recent research proposed a dimensionless shape parameter d/D to suppress the higher-order modes of HC-NCFs, where d is the capillary diameter and D is the hollow core diameter [14]. We also observed that the HC-NCF could exhibit a low fringe noise by optimizing the coupling optics and gas pressure.

We first investigated the transmission background signal with the hollow core filled with ambient air. As illustrated in Fig. 4, two baselines were recorded with different apertures (5.2 mm and 10 mm in diameter) of the iris placed in the optical path. The baseline was fitted by a polynomial function with the fitting residual plotted at the bottom panel of Fig. 4. Though the iris with a smaller aperture reduced the incident laser power, the fringe noise was significantly mitigated shown in Fig. 4(a) by probably avoiding the excitation of higher-order modes. The fringe noise was probably caused by a mismatch between the emission characteristics of the ICL and the fundamental mode field of the hollow core. Note that the excited modes of the hollow core may be affected by the intensity distribution of the incident laser beam [36]. Hence, the iris of 5.2-mm diameter was used in the following sensor development considering the effectively suppressed fringe noise in the optical system.

We also investigated the influence of gas pressure on DAS with HC-NCFs. Fig. 5(a) compares the measured absorbance signal of 4.4% N_2O/N_2 with the Voigt fitting. All the measurements were conducted at different pressures between 0.1 and 1.8 atm. The time-varying fringes could be hardly eliminated by the baseline subtraction method. However, such

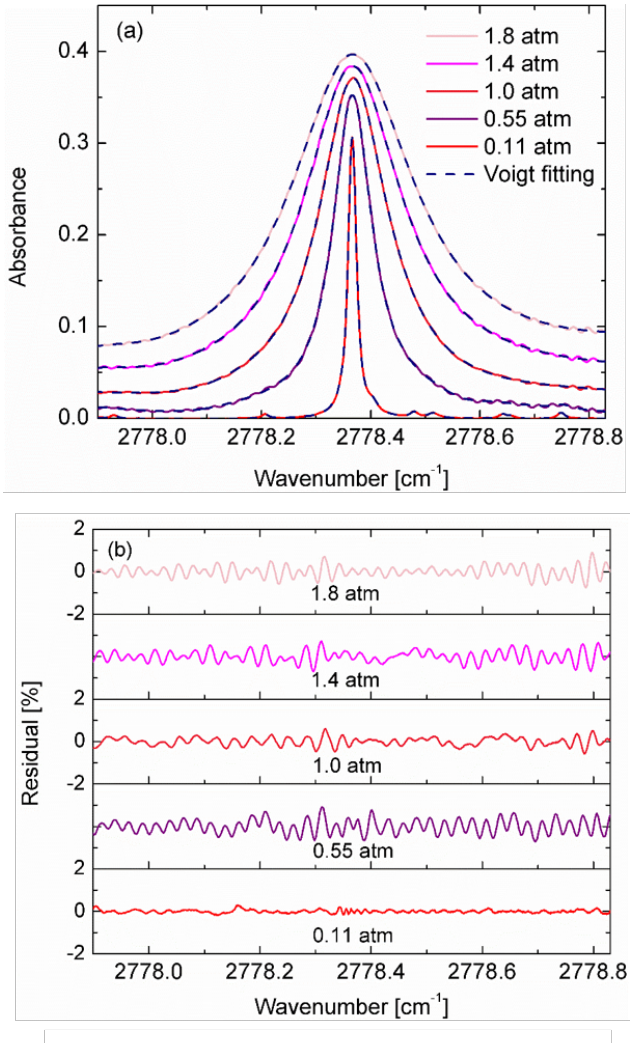

Fig. 5. DAS measurements of 4.4% N_2O at different gas pressures: (a) measured absorbance profiles with the Voigt fitting; (b) fitting residual.

a noise is relevant to gas pressure in the hollow core that the fringe noise appeared much smaller at a low pressure of 0.11 atm shown in Fig. 5(a). Since higher-order modes in the hollow core fiber are relevant to the fiber bending or stress, the change of fringe amplitude may result from the slight deformation of fiber structure at different gas pressures. However, a more systematic research is needed in the future to understand the mechanism. To quantitatively evaluate the fringe noise, Fig. 5(b) presents the fitting residuals of all the measured absorbance data with the Voigt fitting. The fitting residual is within ±0.3 % at 0.11 atm but increases with higher gas pressures. In particular, the fringe noise is reduced by a factor of 5 at 0.11 atm compared with that at 0.55 atm. Hence, we selected 0.11 atm as the operating pressure for the HC-NCF-based DAS detection. Meanwhile, the non-absorbing region within a limited spectral scan was easily attained at a lower pressure, so the baseline could be obtained by directly fitting the transmitted signal with a polynomial function.

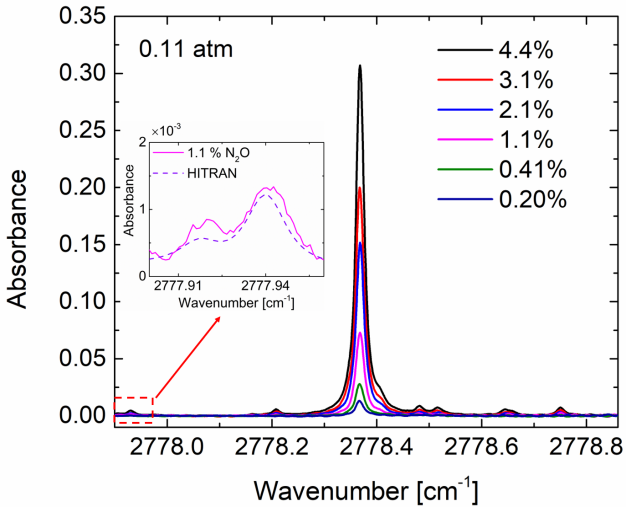

Fig. 6. DAS measurements of different N_2O concentrations at a gas pressure of 0.11 atm. Inset: the weak absorption feature of 1.1% N_2O measured at 2777.9 cm^{-1} (HITRAN simulation is plotted for comparison).

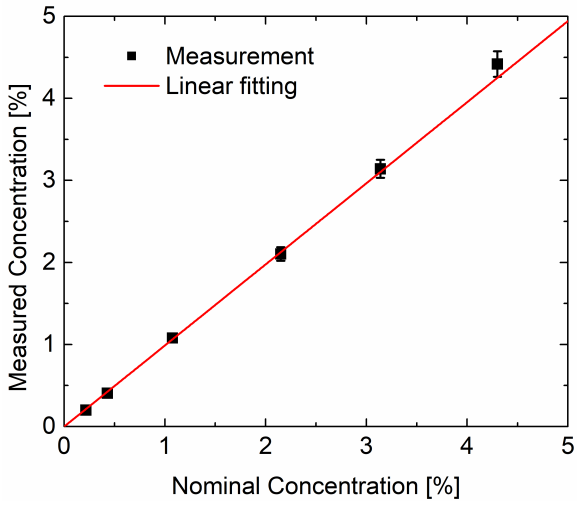

Fig. 7. Comparison of the measured N_2O concentration by the DAS sensor with the nominal value obtained by the gas dilution system.

B. *Detection sensitivity*

Fig. 6 depicts the representative absorption spectra of N_2O/N_2 mixtures measured from 2777.88 cm^{-1} to 2778.9 cm^{-1} at room temperature and pressure of 0.11 atm. Several absorption peaks could be identified in this spectral region. As illustrated in the inset graph of Fig. 6, some weak lines near 2777.94 cm^{-1} of ~ 0.001 absorbance were also identified with a good SNR. The strongest absorption line at 2778.37 cm^{-1} was selected as the target line for N_2O sensitivity determination.

The absorbance data were then fitted by the Voigt line-shape function to determine the integrated area of the absorbance. Thus gas concentration could be directly inferred using Eqn. (3). Fig. 7 plots the measured N_2O concentrations as a function of the nominal values generated from the gas dilution system; and a R-square value of 0.999 was obtained by the linear fitting.

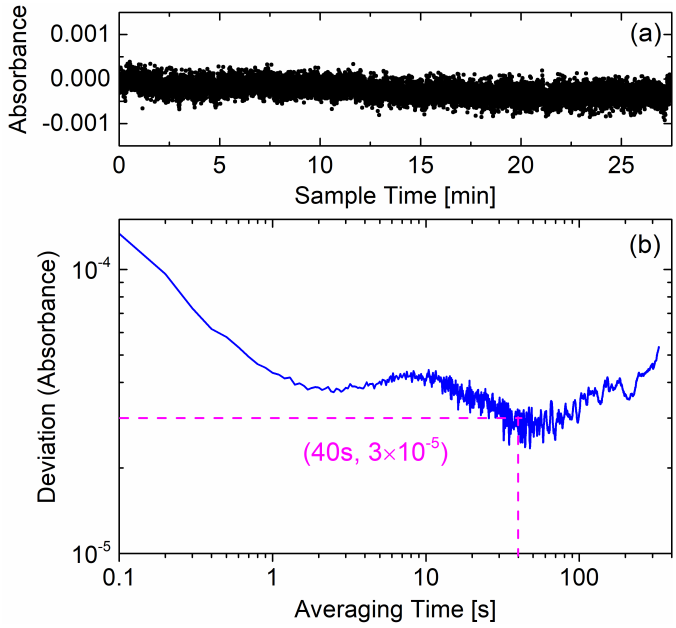

Fig. 8. (a) Continuous DAS measurement of air in the HC-NCF; (b) Allan-Werle deviation analysis in terms of absorbance.

The uncertainty of the measured concentration shown in Fig. 7 is determined by the following factors:

$$\frac{\Delta C}{C} = \left|\frac{\partial \ln C}{\partial A}\right| \cdot \Delta A + \left|\frac{\partial \ln C}{\partial P}\right| \cdot \Delta P + \left|\frac{\partial \ln C}{\partial L}\right| \cdot \Delta L + \left|\frac{\partial \ln C}{\partial S}\right| \cdot \Delta S, \quad (6)$$

where the relative measurement error of pressure (P), fiber length (L) and line-strength (S) are ±1.5%, ±0.5% and ±1% [33], respectively. The uncertainty of the integrated absorbance fitted by the Voigt profile is determined to be between ±0.5% and ±4% for different N_2O concentrations. A signal-to-noise ratio of 57 was obtained for the mixture of 0.2% N_2O, resulting in a minimum detection limit (1-σ) of 35 ppm N_2O for the HC-NCF-based DAS sensor.

The long-term stability of the HC-NCF-based DAS sensor was investigated by the Allan-Werle deviation analysis shown in Fig. 8. In this test ambient air was introduced into the HC-NCF for the continuous measurement with a wavelength scan of 10 Hz. The minimum detectable absorbance for the current system is determined to be 3×10^{-5} at 40 s, corresponding to a NEA coefficient of 2.5×10^{-7} cm^{-1} normalized by the fiber length. Note that the NEA coefficient at the level of 10^{-7} cm^{-1} was never achieved by direct absorption spectroscopy performed with a large core (> 15 μm) HC-MOF [1-3], which was mainly limited by the mode noise. Although it is known that the larger core supports more high-order modes [11], this work demonstrated the low fringe noise achieved by the HC-NCF with a core diameter of 65 μm. Additionally, a larger core diameter are beneficial for fast gas loading that is significant for gas sensor development [7].

V. Conclusion

In this proof-of-principle experiment, we demonstrated a new opportunity of developing mid-infrared gas sensors by combining laser absorption spectroscopy with a novel hollow-core fiber. The anti-resonance HC-NCF fiber has a core size of 65 μm, which is inscribed by a single ring of six nontouching capillaries. An ICL emitting at 3.6 μm was implemented for the high-resolution DAS measurement of N_2O absorption lines. The HC-NCF provided a nearly single-mode transmission with very low transmission loss. The mode interference in the large hollow core was investigated and suppressed by optimizing the laser beam shape and using a low gas pressure. We achieved a minimum detectable absorbance of 3×10^{-5} for a fiber length of 120 cm, corresponding to a NEA coefficient of 2.5×10^{-7} cm^{-1}. The sensing scheme is of interest to detect other gas species at very low concentration in the future.

References

[1] Ł. Kornaszewski, N. Gayraud, J. M. Stone, W. N. Macpherson, A. K. George, J. C. Knight, D. P. Hand, and D. T. Reid, "Mid-infrared methane detection in a photonic bandgap fiber using a broadband optical parametric oscillator," *Opt. Express*, vol. 15, no. 18, pp. 11219–11224, 2007.

[2] M. N. Petrovich, A. M. Heidt, N. V. Wheeler, N. K. Baddela, and D. J. Richardson, "High sensitivity methane and ethane detection using low-loss mid-IR hollow-core photonic bandgap fibers," *23rd Int. Conf. Opt. Fibre Sensors*, vol. 9157, p. 91573, 2014.

[3] J. A. Nwaboh, J. Hald, J. K. Lyngsø, J. C. Petersen, and O. Werhahn, "Measurements of CO_2 in a multipass cell and in a hollow-core photonic bandgap fiber at 2 μm," *Appl. Phys. B Lasers Opt.*, vol. 110, no. 2, pp. 187–194, 2013.

[4] Y. L. Hoo, S. Liu, H. L. Ho, and W. Jin, "Fast response microstructured optical fiber methane sensor with multiple side-openings," *IEEE Photonics Technol. Lett.*, vol. 22, no. 5, pp. 296–298, 2010.

[5] A. M. Cubillas, M. Silva-Lopez, J. M. Lazaro, O. M. Conde, M. N. Petrovich, and J. M. Lopez-Higuera, "Methane detection at 1670-nm band using a hollow-core photonic bandgap fiber and a multiline algorithm," *Opt. Express*, vol. 15, no. 26, pp. 17570–17576, 2007.

[6] F. Yang, W. Jin, Y. Cao, H. L. Ho, and Y. Wang, "Towards high sensitivity gas detection with hollow-core photonic bandgap fibers," *Opt. Express*, vol. 22, no. 20, pp. 24894–24907, 2014.

[7] M. Nikodem, G. Gomółka, M. Klimczak, D. Pysz, and R. Buczyński, " Laser absorption spectroscopy at 2 μm inside revolver-type anti-resonant hollow core fiber," *Opt. Express*, vol. 27, no. 10, pp. 14998–15006, 2019.

[8] L. Hu, C. Zheng, D. Yao, D. Yu, Z. Liu, J. Zheng, Y. Wang, and F. K. Tittel, "A hollow-core photonic band-gap fiber based methane sensor system capable of reduced mode interference noise," *Infrared Phys. Technol.*, vol. 97, pp. 101–107, 2019.

[9] W. Jin, Y. Cao, F. Yang, and H. L. Ho, "Ultra-sensitive all-fibre photothermal spectroscopy with large dynamic range," *Nat. Commun.*, vol. 6, pp. 1–8, 2015.

[10] C. Yao, Q. Wang, Y. Lin, W. Jin, L. Xiao, S. Gao, Y. Wang, P. Wang, and W. Ren, "Photothermal CO detection in a hollow-core negative curvature fiber," *Opt. Lett.*, vol. 44, no. 16, pp. 4048–4051, 2019.

[11] M. N. Petrovich, F. Poletti, A. Van Brakel, and D. J. Richardson, "Robustly single mode hollow core photonic bandgap fiber," *Opt. Express*, vol. 16, no. 6, pp. 4337–4346, 2008.

[12] Y. Wang and W. Ding, "Confinement loss in hollow-core negative curvature fiber: A multi-layered model," *Opt. Express*, vol. 25, no. 26, pp. 33122–33133, 2017.

[13] B. Debord, A. Amsanpally, M. Chafer, A. Baz, M. Maurel, J. M. Blondy, E. Hugonnot, F. Scol, L. Vincetti, F. Gérôme, and F. Benabid, "Ultralow transmission loss in inhibited-coupling guiding hollow fibers," *Optica*, vol. 4, no. 2, pp. 209–217, 2017.

[14] P. Uebel, M. C. Günendi, M. H. Frosz, G. Ahmed, N. N. Edavalath, J. M. Ménard, and P. S. J. Russell, "Broadband robustly single-mode hollow-core PCF by resonant filtering of higher-order modes," *Opt. Lett.*, vol. 41, no. 9, pp. 1961–1964, 2016.

[15] S. Gao, Y. Wang, W. Ding, D. Jiang, S. Gu, X. Zhang, and P. Wang, "Hollow-core conjoined-tube negative-curvature fibre with ultralow loss," *Nat. Commun.*, vol. 9, no. 1, p. 2828, 2018.

[16] C. Gong, Y. Gong, Q. Chen, Y. Rao, G. Peng, and X. Fan, "Reproducible fiber optofluidic laser for disposable and array applications," *Lab Chip*, vol. 17, no. 20, pp. 3431–3436, 2017.

[17] J. Yu, Y. Liu, Y. Wang, Z. Wang, X. Zhang, X. Liu, S. Gao, X. Wang and P. Wang, "Optofluidic laser based on a hollow-core negative-curvature fiber," *Nanophotonics*, vol. 7, no. 7, pp.1307–1315, 2018.

[18] C. Gong, Y. Gong, X. Zhao, Y. Luo, Q. Chen, X. Tan, Y. Wu, X. Fan, G. Peng, Y. Rao, "Distributed fibre optofluidic laser for chip-scale arrayed biochemical sensing," *Lab Chip*, vol. 18, no. 18, pp.2741–2748, 2018.

[19] F. Yu, W. J. Wadsworth, and J. C. Knight, "Low loss silica hollow core fibers for 3-4 μm spectral region," *Opt. Express*, vol. 20, no. 10, pp. 11153–11158, 2012.

[20] S. Gao, Y. Wang, and P. Wang, "Silica-based nodeless hollow-core fiber for broadband mid-IR guidance," in *2017 Conference on Lasers and Electro-Optics Pacific Rim (CLEO-PR)*, 2017, pp. 1–2.

[21] A. D. Pryamikov, A. S. Biriukov, A. F. Kosolapov, V. G. Plotnichenko, S. L. Semjonov, and E. M. Dianov, "Demonstration of a waveguide regime for a silica hollow-core microstructured optical fiber with a negative curvature of the core boundary in the spectral region > 3.5 μm," *Opt. Express*, vol. 19, no. 2, pp. 1441–1448, 2011.

[22] W. Belardi and J. C. Knight, "Hollow antiresonant fibers with low bending loss," *Opt. Express*, vol. 22, no. 8, pp. 10091–10096, 2014.

[23] J. D. Shephard, W. N. MacPherson, R. R. J. Maier, J. D. C. Jones, D. P. Hand, M. Mohebbi, A. K. George, P. J. Roberts, and J. C. Knight, "Single-mode mid-IR guidance in a hollow-core photonic crystal fiber," *Opt. Express*, vol. 13, no. 18, pp. 7139–7144, 2005.

[24] A. Urich, R. R. J. Maier, B. J. Mangan, S. Renshaw, J. C. Knight, D. P. Hand, and J. D. Shephard, "Delivery of high energy Er:YAG pulsed laser light at 2 . 94 μm through a silica hollow core photonic crystal fibre," *Opt. Express*, vol. 20, no. 6, pp. 9160–9167, 2012.

[25] N. V Wheeler, A. M. Heidt, N. K. Baddela, E. N. Fokoua, J. R. Hayes, S. R. Sandoghchi, F. Poletti, M. N. Petrovich, and D. J. Richardson, "Low-loss and low-bend-sensitivity mid-infrared guidance in a hollow-core-photonic-bandgap fiber," *Opt. Lett.*, vol. 39, no. 2, pp. 295–298, 2014.

[26] M. I. Hasan, N. Akhmediev, and W. Chang, "Mid-infrared supercontinuum generation in supercritical xenon-filled hollow-core negative curvature fibers," *Opt. Lett.*, vol. 41, no. 21, pp. 5122–5125, 2016.

[27] M. Cassataro, D. Novoa, M. C. Günendi, N. N. Edavalath, M. H. Frosz, J. C. Travers, and P. S. J. Russell, "Generation of broadband mid-IR and UV light in gas-filled single-ring hollow-core PCF," *Opt. Express*, vol. 25, no. 7, pp. 7637–7644, 2017.

[28] L. Cao, S. Gao, Z. Peng, X. Wang, Y. Wang, and P. Wang, "High peak power 2.8 μm Raman laser in a methane-filled negative-curvature fiber," *Opt. Express*, vol. 26, no. 5, pp. 5609–5615, 2018.

[29] A. V. Gladyshev, A. F. Kosolapov, M. M. Khudyakov, Y. P. Yatsenko, A. N. Kolyadin, A. A. Krylov, A. D. Pryamikov, A. S. Biriukov, M. E. Likhachev, and I. Bufetov, "4.4-μm Raman laser based on hollow-core silica fibre," *Quantum Electron.*, vol. 47, no. 5, p. 491, 2017.

[30] R. K. Hanson, R. M. Spearrin, and C. S. Goldenstein, Spectroscopy and optical diagnostics for gases. Springer, 2016.

[31] J. Humlíček, "Optimized computation of the Voigt and complex probability functions," *J. Quant. Spectrosc. Radiat. Transf.*, vol. 27, no. 4, pp. 437–444, 1982.

[32] C. Yao, Q. Wang, Y. Lin, W. Jin, L. Xiao, S. Gao, Y. Wang, P. Wang, and W. Ren, "Photothermal CO detection in a hollow-core negative curvature fiber," *Opt. Lett.*, vol. 44, no. 16, pp. 4048–4051, 2019.

[33] I. E. Gordon, L. S. Rothman, C. Hill, R. V. Kochanov, Y. Tan, P. F. Bernath, M. Birk, V. Boudon, A. Campargue, K. V. Chance, B. J. Drouin, J. M. Flaud, R. R. Gamache, J. T. Hodges, D. Jacquemart, V. I. Perevalov, A. Perrin, K. P. Shine, M. A. H. Smith, J. Tennyson, G. C. Toon, H. Tran, V. G. Tyuterev, A. Barbe, A. G. Császár, V. M. Devi, T. Furtenbacher, J. J. Harrison, J. M. Hartmann, A. Jolly, T. J. Johnson, T. Karman, I. Kleiner, A. A. Kyuberis, J. Loos, O. M. Lyulin, S. T. Massie, S. N. Mikhailenko, N. Moazzen-Ahmadi, H. S. P. Müller, O. V. Naumenko, A. V. Nikitin, O. L. Polyansky, M. Rey, M. Rotger, S. W. Sharpe, K. Sung, E. Starikova, S. A. Tashkun, J. Vander Auwera, G. Wagner, J. Wilzewski, P. Wcisło, S. Yu, and E. J. Zak, "The HITRAN2016 molecular

spectroscopic database," *J. Quant. Spectrosc. Radiat. Transf.*, vol. 203, pp. 3–69, 2017.

[34] Z. Wang, Z. Li, W. Ren, and H. Kong, "Quartz-enhanced photoacoustic detection of ethylene using a 10.5 um quantum cascade laser," *Opt. Express*, vol. 24, no. 4, pp. 4143–4154, 2016.

[35] N.L.P. Andrews, R. Ross, D. Munzke, C. van Hoorn, A. Brzezinski, J.A. Barnes, O. Reich, H.-P. Loock, "In-fiber Mach-Zehnder interferometer for gas refractive index measurements based on a hollow-core photonic crystal fiber," *Opt. Express*. vol. 24, no. 13, pp.14086–14099, 2016.

[36] T. G. Euser, G. Whyte, M. Scharrer, J. S. Y. Chen, A. Abdolvand, J. Nold, C. F. Kaminski, and P. S. J. Russell, "Dynamic control of higher-order modes in hollow-core photonic crystal fibers," *Opt. Express*, vol. 16, no. 22, pp. 17972–17981, 2008.